Remote Sensing Of Environment
June 2018, Volume 211 Pages 13-25
https://doi.org/10.1016/j.rse.2018.03.038
https://archimer.ifremer.fr/doc/00436/54725/

LiDAR derived forest structure data improves predictions of canopy N and P concentrations from imaging spectroscopy

Ewald Michael [1, *], Aerts Raf [2], Lenoir Jonathan [3], Fassnacht Fabian Ewald [1], Nicolas Manuel [4], Skowronek Sandra [5], Piat Jerome [4], Honnay Olivier [2], Garzon-Lopez Carol Ximena [3, 6], Feilhauer Hannes [5], Van De Kerchove Ruben [7], Somers Ben [8], Hattab Tarek [3, 9], Rocchini Duccio [10, 11, 12], Schmidtlein Sebastian [1]

[1] Karlsruhe Inst Technol, Inst Geog & Geoecol, Kaiserstr 12, D-76131 Karlsruhe, Germany.
[2] Katholieke Univ Leuven, Biol Dept, Kasteelpk Arenberg 31-2435, B-3001 Leuven, Belgium.
[3] Univ Picardie Jules Verne, UMR CNRS 7058, EDYSAN, UR Ecol & Dynam Syst Anthropises, 1 Rue Louvels, F-80037 Amiens 1, France.
[4] Off Natl Forets, Dept Rech & Dev, F-77300 Fontainebleau, France.
[5] FAU Erlangen Nuremberg, Inst Geog, Wetterkreuz 15, D-91058 Erlangen, Germany.
[6] Univ Los Andes, Ecol & Vegetat Physiol Grp EcoFiv, Cr 1E 18A, Bogota, Colombia.
[7] VITO Flemish Inst Technol Res, Boeretang 200, B-2400 Mol, Belgium.
[8] Katholieke Univ Leuven, Dept Earth & Environm Sci, Celestijnenlaan 200E, B-3001 Leuven, Belgium.
[9] Inst Francais Rech Exploitat Mer, UMR MARBEC, Ave Jean Monnet CS, Sete, France.
[10] Fdn Edmund Mach, Res & Innovat Ctr, Dept Biodivers & Mol Ecol, Via E Mach 1, I-38010 San Michele All Adige, TN, Italy.
[11] Univ Trento, Ctr Agr Food Environm, Via E Mach 1, I-38010 San Michele All Adige, TN, Italy.
[12] Univ Trento, Ctr Integrat Biol, Via Sommarive 14, I-38123 Povo, TN, Italy.

* Corresponding author : Michael Ewald, email address : michael.ewald@kit.edu

Abstract :

Imaging spectroscopy is a powerful tool for mapping chemical leaf traits at the canopy level. However, covariance with structural canopy properties is hampering the ability to predict leaf biochemical traits in structurally heterogeneous forests. Here, we used imaging spectroscopy data to map canopy level leaf nitrogen (Nmass) and phosphorus concentrations (Pmass) of a temperate mixed forest. By integrating predictor variables derived from airborne laser scanning (LiDAR), capturing the biophysical complexity of the canopy, we aimed at improving predictions of Nmass and Pmass. We used partial least squares regression (PLSR) models to link community weighted means of both leaf constituents with 245 hyperspectral bands (426–2425 nm) and 38 LiDAR-derived variables. LiDAR-derived variables improved the model's explained variances for Nmass (R2cv 0.31 vs. 0.41, % RSMEcv 3.3 vs. 3.0) and Pmass (R2cv 0.45 vs. 0.63, % RSMEcv 15.3 vs. 12.5). The predictive performances of Nmass models using hyperspectral bands only, decreased with increasing structural heterogeneity included in the calibration dataset. To test the independent contribution of canopy structure we additionally fit the models using only LiDAR-derived variables as predictors. Resulting R2cv values ranged from 0.26 for Nmass to 0.54 for Pmass indicating considerable covariation between biochemical traits and forest structural properties. Nmass was negatively related to the spatial heterogeneity of canopy density, whereas Pmass was

negatively related to stand height and to the total cover of tree canopies. In the specific setting of this study, the importance of structural variables can be attributed to the presence of two tree species, featuring structural and biochemical properties different from co-occurring species. Still, existing functional linkages between structure and biochemistry at the leaf and canopy level suggest that canopy structure, used as proxy, can in general support the mapping of leaf biochemistry over broad spatial extents.

Highlights

► LiDAR data improves predictive models of canopy N and P using imaging spectroscopy. ► Results indicate high covariation between leaf biochemicals and canopy structure. ► Structural properties can support mapping canopy N and P.

Keywords : Remote sensing, Canopy biochemistry, APEX, Hyperspectral imagery, Leaf traits, Leaf nutrient content, Data fusion, Forest ecosystem

1 Introduction

Plant traits are important indicators of ecosystem functioning and are widely used in ecological research to detect responses to environmental change (Chapin, 2003; Garnier et al., 2007; Kimberley et al., 2014) or to quantify ecosystem services (Lamarque et al., 2014; Lavorel et al., 2011). Biochemical traits like leaf nitrogen and phosphorus content respond to changing environmental conditions, such as soil nutrients or climate (Di Palo and Fornara, 2015; Sardans et al., 2015) and are key factors related to important ecological processes including net primary production and litter deiosition (Melillo et al., 1982; Ollinger et al., 2002; Reich, 2012). Temporal trends, like increasing N:P ratios caused by nitrogen deposition can serve as indicators for ecosystem health and sustainability (Jonard et al., 2015; Talkner et al., 2015). Using leaf traits to answer questions related to ecosystem functioning often requires scaling from the leaf to the plant community or ecosystem level (Masek et al., 2015; Suding et al., 2008). Due to the fact that certain leaf biochemical traits are closely linked to the reflectance signature of leaves (Kokaly et al., 2009) the use of imaging spectroscopy has proved to be an efficient method for scaling and the prediction of these traits across large spatial scales (Homolová et al., 2013). By far, most studies relating foliage biochemistry to airborne imaging spectroscopy data

focused on leaf nitrogen (e.g. Dahlin et al., 2013; Huber et al., 2008; Martin and Aber, 1997; Wang et al., 2016). But also other biochemical leaf ingredients like chlorophyll, cellulose and lignin (Curran et al., 1997; Schlerf et al., 2010; Serrano et al., 2002) and even micronutrients like iron and copper (Asner et al., 2015; Pullanagari et al., 2016) have been successfully related to imaging spectroscopy data. Compared to leaf nitrogen, mapping of leaf phosphorus concentrations received less attention (but see Asner et al., 2015; Porder et al., 2005; Pullanagari et al., 2016).

The link between leaf biochemistry and reflectance established in optical remote sensing applications strongly depends on the observational level. At the leaf level, nitrogen concentrations, for example, are directly expressed in the spectral signal. For dried and ground samples, characteristic absorption features can be found in the shortwave infrared (SWIR) region of the electromagnetic spectrum. The absorption of radiation in the SWIR can be attributed to nitrogen bonds in organic compounds primarily of leaf proteins (Kokaly et al., 2009). In fresh leaves the nitrogen concentration is additionally strongly related to absorption in the visible part of the spectrum (VIS) (Asner and Martin, 2008), which can be attributed to the correlation between chlorophyll and leaf nitrogen (Homolová et al., 2013; Ollinger, 2011). At the canopy level, spectral reflectance is strongly influenced by canopy structure (Asner, 1998; Gerard and North, 1997; Rautiainen et al., 2004). Thus, the estimation of leaf traits from canopy reflectance is more complex due to the confounding effects of structural properties like crown morphology, leaf area index (LAI), leaf clumping or stand height (Ali et al., 2016; Simic et al., 2011; Xiao et al., 2014). Consequently, variability in canopy structure can strongly influence the accuracy of nitrogen estimations from remote sensing (Asner and Martin, 2008). On the other hand, canopy structure has been found to explain part of the relation between reflectance and canopy nitrogen. This relation is revealed by a strong importance of reflectance in the near infrared (NIR) for mapping canopy nitrogen reported by previous studies (Martin et al., 2008; Ollinger et al., 2008). Reflection in the NIR region is dominated by multiple scattering between leaves of the canopy, and thus very sensitive to variation in canopy structure (Knyazikhin et al., 2013; Ollinger, 2011). Covariation between canopy structure and nitrogen was found across different types of forest ecosystems and hence points at the existence of a functional link between canopy structure and biochemical composition. However, the foundation of this functional link has not been fully understood.

In this study, we aim at scaling leaf level measurements of mass based leaf nitrogen (N_{mass}) and phosphorus content (P_{mass}) to the canopy scale for a temperate mixed forest. To capture the forest's diversity in terms of tree species, age distribution and canopy structure we propose to explicitly integrate information on forest structure derived from airborne laser scanning (Light Detection And Ranging, LiDAR) into the empirical models. Airborne LiDAR data can depict the 3D structure of the vegetation and has been successfully used to map forest attributes like the leaf area index and standing biomass (Fassnacht et al., 2014; Korhonen et al., 2011; Zolkos et al., 2013). The benefit of LiDAR-derived information on forest structure for mapping of canopy biochemistry has not been assessed yet. We argue that the integration of structural properties allows for a better acquisition of leaf chemical traits in heterogeneous forests canopies. We furthermore

expect that LiDAR data can help to understand expected covariation between canopy structural properties and biochemical leaf traits. Specifically, we aim at: (1.) improving predictions of N_{mass} and P_{mass} using imaging spectroscopy through the integration of LiDAR-derived information on forest structure and (2.) finding out which structural canopy properties correlate with N_{mass} and P_{mass} in canopies of mixed forests.

2 Materials and Methods

2.1 Study area

The study area is the forest of Compiègne (northern France, 49.370° N, 2.886° E), covering an area of 144.2 km^2. This lowland forest is located in the humid temperate climate zone with a mean annual temperature of 10.3°Cand mean annual precipitation of 677 mm. The soils cover a range from acidic nutrient-poor sandy soils to basic and hydromorphic soils (Closset-Kopp et al., 2010). The forest mainly consists of even-aged managed stands of beech (*Fagus sylvatica*), oaks (*Quercus robur*, *Quercus petraea*) and pine (*Pinus sylvestris*) growing in mono-culture as well as in mixed stands, frequently intermingled with European hornbeam (*Carpinus betulus*) and ash (*Fraxinius excelsior*) (Chabrerie et al., 2008). Stands are covering a range from early pioneer stages to more than 200-year-old mature forests. As a result of thinning activities and windthrow the forest is characterized by frequent canopy gaps which are often filled by the American black cherry (*Prunus serotina*), an alien invasive tree species in central Europe. *Prunus serotina* is in some parts also highly abundant in the upper canopy of earlier pioneer stages.

2.2 Field data

Field data were acquired from 50 north-facing field plots (25 m × 25 m) established in July 2014. Of those plots, 44 plots were randomly selected from an initial set of 64 field plots established in 2004 during a previous field study by Chabrerie et al. (2008). Six additional plots were selected to include stands in earlier stages of forest succession, aiming to cover the entire range of structural canopy complexity. The plots covered all main forest stand types including mixed tree species stands in different age classes (supplementary material, Tab. S1). In each plot we recorded the diameter at breast height for all trees and shrubs higher than 2 m.

In July 2015, we sampled leaves from the most abundant tree species making up at least 80% of the basal area in one plot. This resulted in up to five sampled species per plot. For each species in each plot, we took three independent samples, if possible from different individuals. Taller trees were sampled by shooting branches using shotguns (Marlin Model 55 Goose, Marlin Firearms Co, Madison, USA and Winchester Select Sporting II 12M, Winchester, Morgan, USA) with Buckshot 27 ammunition (27 × 6.2 mm pellets), aiming at single branches (Aerts et al., 2017). Samples from smaller trees were taken using a pole clipper. In both cases leaves from the upper part of the crown were preferably chosen. Trees growing in canopy gaps were sampled in the center of these

gaps, in order to collect the most sunlit leaves from these individuals. For broadleaved trees, each sample consisted of 10 to 15 undamaged leaves, depending on leaf size. The samples of the only coniferous tree species *P. sylvestris* consisted of at least 20 needles from both the current and the last growing season. In total, we collected 328 leaf samples from nine different tree species. Leaves were put in sealed plastic bags and stored in cooling boxes. At the end of each field day samples were weighed, and then dried at 80°C for 48 hours.

Back from the field, leaves were milled prior to the analysis. N_{mass} was measured applying the Dumas method using a vario MACRO element analyzer (Elementar Analysensysteme, Hanau, Germany). P_{mass} was measured using an inductively coupled plasma-optical emission spectrometer (ICP-OES) (Varian 725ES, Varian Inc., Palo Alto, CA, USA). For each field plot, we calculated community weighted mean values for N_{mass} and P_{mass}, taking the basal area of each species in the corresponding plot as the weight. The relative basal area is a good approximation for relative canopy cover of the tree species co-occurring in a forest stand (Cade, 1997; Gill et al., 2000). The relative canopy cover corresponds to the contribution of each species to the reflectance signal of a mixed forest canopy. Although field samples were collected one year after the acquisition of remote sensing data, we consider our field data set as a solid basis for the prediction of N_{mass} and P_{mass}. Previous studies indicate that in temperate tree species there are no remarkable differences in leaf chemical contents between two consecutive years (Reich et al., 1991; Smith et al., 2003). Furthermore, N_{mass} in deciduous broadleaved species typically shows only little variation during the mid-growing season (McKown et al., 2013; Niinemets, 2016; Reich et al., 1991) and remains stable under drought conditions (Grassi et al., 2005; Wilson et al., 2000). The latter point is noteworthy, because the early summer of 2015 was dryer compared to the year 2014.

2.3 Remote sensing data

We used airborne imaging spectroscopy data (284 bands, 380 nm – 2500 nm) acquired by the Airborne Prism Experiment (APEX) spectrometer with a spatial resolution of 3 m × 3 m, and airborne discrete return LiDAR data with an average point density of 23 points per m^2, both covering the entire study area. APEX data were acquired on July 24, 2014 (9:56 – 11:25 UTC + 2h) at a flight height of 5400 m by the Flemish Institute of Technology (VITO, Mol, Belgium). The data, consisting of 12 flight lines, were delivered geometrically and atmospherically corrected using the standard processing chain applied to APEX recorded images (Sterckx et al., 2016; Vreys et al., 2016). Bands from both ends of the spectra and bands disturbed by water absorption were deleted prior to the analysis. In total, we included 245 spectral bands between 426 nm and 2425 nm for subsequent analyses. We applied a Normalized Differenced Vegetation Index (NDVI) mask in order to exclude values from pixels with bare soil and ground vegetation (Asner et al., 2015). For this purpose, we calculated NDVI values for each pixel and excluded pixels with a NDVI below 0.75. For all remaining pixels we applied a brightness normalization to reduce the influence of canopy shades on the spectral signal (Feilhauer et al., 2010).

LiDAR points were recorded in February 2014 at leaf-off conditions by Aerodata (Lille,

France) using a Riegl LMS-680i with a maximum scan angle of 30°and a lateral overlap of neighboring flight lines of 65%. Average flight height during LiDAR data acquisition was 530 m resulting in a beam diameter of about 0.265 m. The LiDAR data were delivered including a classification of ground and vegetation returns and a digital terrain model (DTM). Height values of LiDAR points were normalized, by subtracting values of the underlying DTM. Vegetation returns were then aggregated into a grid with a cell size of 3 m × 3 m, taking the grid matrix of the imaging spectroscopy data as reference. For each pixel we calculated 19 different LiDAR-derived variables based on point statistics resulting in 19 raster layers. Calculated LiDAR-derived variables included basic summary statistics (e.g. maximum height) based on the height values of LiDAR points in each grid cell and inverse penetration ratios representing the fractional vegetation cover within given height thresholds (Tab. 1) (Ewald et al., 2014). Penetration ratios were calculated using the following formula:

$$vc_{h12} = (n_{h2} - n_{h1})/n_{h2} \tag{1}$$

where vc_{h12} is representing the vegetation cover within the height thresholds h1 and h2 (h1 < h2) within one grid cell. n_{h1} and n_{h2} represent the sum of all LiDAR points below the given height thresholds h1 and h2, respectively.

Table 1 Variables calculated from LiDAR point clouds in 3 m × 3 m resolution. For the use in partial least squares regression models, variables were aggregated into a grid with a cell size of 24 m × 24 m, by calculating mean and standard deviation.

LiDAR Metric	**Abbreviation**	**Description**
Minimum	min_h_mean; min_h_sd	Basic statistics
Maximum	max_h_mean; max_h_sd	based on the
Mean	mean_h_mean; mean_h_sd	height values of
Standard deviation	sd_h_mean; sd_h_sd	vegetation LiDAR
Variance	var_h_mean; var_h_sd	points
Coefficient of variation	cov_h_mean; cov_h_sd	
10th percentile	perc10_h_mean; perc10_h_sd	
25th percentile	perc25_h_mean; perc25_h_sd	
50th percentile	perc50_h_mean; perc50_h_sd	
75th percentile	perc75_h_mean; perc75_h_sd	
90th percentile	perc90_h_mean; perc90_h_sd	
Fractional cover 0.5m – 2m	fcover_05_2_mean; fcover_05_2_sd	Inverse penetration
Fractional cover 0.5m – 60m	fcover_05_60_mean; fcover_05_60_sd	ratios representing
Fractional cover 2m – 6m	fcover_2_6_mean; fcover_2_6_sd	an estimate for
Fractional cover 2m – 60m	fcover_2_60_mean; fcover_2_60_sd	fractional cover of
Fractional cover 6m – 10m	fcover_6_10_mean; fcover_6_10_sd	the vegetation
Fractional cover 6m – 60m	fcover_6_60_mean; fcover_6_60_sd	within given height
Fractional cover 10m – 20m	fcover_10_20_mean; fcover_10_20_sd	thresholds
Fractional cover 20m – 60m	fcover_20_60_mean; fcover_20_60_sd	

From both imaging spectroscopy and LiDAR raster layers, we extracted values from all pixels overlapping with the 50 field plots to be used as input to the statistical models. For each plot, we calculated the weighted mean values of 245 hyperspectral bands and

19 LiDAR-variables (Tab. 1) from the extracted cell values, using the percent overlap of each cell with the plot area as weight. Similarly, we calculated the weighted standard deviation for LiDAR-derived variables which represent a measure of spatial heterogeneity of these variables.

For prediction we aggregated the pixels of the imaging spectroscopy and LiDAR raster layers to a grid with a pixel size of 24 m × 24 m, calculating the mean and the standard deviation (for LiDAR-derived variables only) of all aggregated cells. This finally resulted in a dataset containing 245 spectral bands and 38 LiDAR-derived variables (mean and standard deviation).

2.4 Model calibration and validation

For both response variables, N_{mass} and P_{mass}, we built predictive models using the extracted values from the raster layers at plot locations as predictors. We calculated partial least squares regression (PLSR) models with a step-wise backward model selection procedure implemented in the R package autopls (R Core Team, 2016; Schmidtlein et al., 2012). The number of latent variables was chosen based on the lowest root mean squared error (RMSE) in leave-one-out cross-validation. Before model calibration predictors were normalized, dividing each predictor variable by its standard deviation.

To test the benefit of LiDAR-derived data for the prediction of community weighted means of N_{mass} and P_{mass} at the canopy level we fit two sets of models for each response variable, one incorporating the hyperspectral bands only and a second one using a combination of hyperspectral bands and LiDAR-derived variables as predictors. To test the independent contribution of LiDAR data on the predictions, we additionally fit a third set of models for both N_{mass} and P_{mass} including only LiDAR-derived variables as predictors. N_{mass} values were natural log transformed prior to the model calculations.

The model calculations and predictions were embedded in a resampling procedure with 200 permutations, in order to reduce the bias in model predictions, yielding to a better comparison between the three sets of models. In each permutation, a subsample of 40 out of the 50 field plots was randomly drawn without replacement and used for model calibration and validation. Each model was used to generate a prediction map with a grid size of 24 m × 24 m, resulting in 200 prediction maps for each response variable and each of the three predictor combinations used, respectively. From these maps we calculated a median prediction map and the associated coefficient of variation (CV), representing the spatial uncertainty of model predictions (Singh et al., 2015).

For the assessment of the predictive performance of the models, we calculated the mean Pearson r-squared as well as the absolute and normalized root mean squared error (RMSE) between predicted and observed values of each data subset. The same performance measures were calculated for each data subset in leave-one-out cross-validation data. For N_{mass}, r-squared values and RMSE were calculated based on the log-transformed dataset. The normalized RMSE was calculated by dividing the RMSE by the mean value in the response dataset. r-squared and RMSE values were used to compare the performances of models using only hyperspectral bands or a combination of hyperspectral bands and LiDAR-derived variables as predictors, for N_{mass} and P_{mass} respectively.

Model performance is affected by the number of variables included, in the case of a PLSR the number of latent variables. To check for such an effect we grouped the corresponding models according to the number of latent variables included and compared the r-squared values for each group separately (supplementary material, Fig. S1).

3 Results

Field plots were located in forest stands with heights ranging from 3 to 40 m and LAI values ranging from 1.7 to 5.9 (supplementary material, Tab. S2). Plot-wise community weighted mean values for N_{mass} and P_{mass} ranged from 13.8 to 25.4 g·kg^{-1} and from 0.82 to 1.93 g·kg^{-1}, respectively. N_{mass} of *P. serotina* and *P. sylvestris* were significantly different from all other species (supplementary material, Fig. S2 and, Tab. S3). Contrary, we observed no differences in measured N_{mass} between. *F. sylvatica*, *Q. robur* and *C. betulus*. P_{mass} differed significantly between all species except between *C. betulus* and *Q. robur* (supplementary material, Fig. S2). Models combining structural vegetation attributes, derived from airborne LiDAR, with imaging spectroscopy improved predictions of community weighted mean values for N_{mass} and P_{mass} compared to models using imaging spectroscopy data solely (Tab. 2, Fig. 2). In the combined N_{mass} models, hyperspectral bands had a significantly higher contribution ($p < 0.001$) to the variance explained, compared to LiDAR-derived variables (Fig. 1). By contrast, in P_{mass} models, LiDAR-derived variables showed a significantly higher contribution ($p < 0.001$). With respect to the selected spectral bands we observed only marginal differences between models including LiDAR-derived variables and models not including them (Figs. 3, 4, 5, 6).

Table 2 Results of PLSR models for N_{mass} and P_{mass} from 200 bootstraps. Predictors: used predictor variables being either, hyperspectral bands (HS) or LiDAR-derived variables; # LV: mean number of latent variables; # Var: mean number of selected predictor variables; R^2_{cal}: mean coefficient of determination in calibration; R^2_{cv}: mean coefficient of determination in validation; $RMSE_{cal}$: average root mean squared error in calibration; $RMSE_{cv}$: average root mean squared error in leave-one-out cross-validation

Response	Predictors	#LV	#Var	R^2_{cal}	R^2_{cv}	RMSE$_{cal}$	RMSE$_{cv}$	RMSE$_{cal}$ [%]	RMSE$_{cv}$ [%]
N_{mass}*	HS	5.8	98	0.47 ± 0.10	0.31 ± 0.14	0.09 ± 0.01	0.09 ± 0.01	2.9	3.3
	HS & LiDAR	5.7	43	0.55 ± 0.12	0.41 ± 0.16	0.08 ± 0.01	0.09 ± 0.01	2.7	3.0
	LiDAR	3.5	8	0.39 ± 0.08	0.26 ± 0.09	0.09 ± 0.01	0.10 ± 0.01	3.1	3.4
P_{mass}	HS	6.3	42	0.59 ± 0.15	0.45 ± 0.16	0.15 ± 0.02	0.18 ± 0.02	13.1	15.3
	HS & LiDAR	6.9	38	0.73 ± 0.08	0.63 ± 0.10	0.13 ± 0.02	0.14 ± 0.02	10.8	12.5
	LiDAR	3.7	9	0.62 ± 0.08	0.54 ± 0.10	0.15 ± 0.01	0.17 ± 0.01	12.6	14.0

∗natural log-transformed

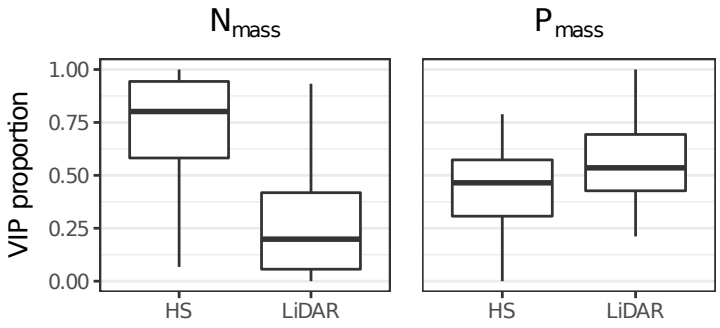

Figure 1 Relative contribution of hyperspectral bands (HS) and LiDAR variables to the variance explained in PLSR models for N_{mass} and P_{mass} expressed as proportion of the total VIP (Variable Importance in Projection) score.

For N_{mass} the average R^2_{cv} values resulting from leave-one-out cross-validation for each bootstrap model increased from 0.31 to 0.41 whereas the mean relative RSME decreased only moderately (see Tab. 2) when adding LiDAR-derived variables. Models fitted by LiDAR-derived predictors solely resulted in a mean R^2_{val} value of 0.25. The most important LiDAR-derived variables in the models predicting of N_{mass} were, according to VIP values, related to the horizontal variation of canopy cover (fcover_05_60_sd, fcover_2_6_sd, fcover_6_10_sd, fcover_6_60_sd) (Figs. 7, 8). The most important spectral bands were located in the VIS and the SWIR between 2000 and 2400 nm, irrespective of whether only imaging spectroscopy or a combination of imaging spectroscopy and LiDAR data was used (Fig. 3).

For P_{mass}, average R^2_{cv} values resulting from leave-one-out cross-validation for each bootstrap model increased from 0.45 to 0.63 and the mean relative RSME decreased from 15.3 to 12.5 (see Tab. 2), when LiDAR-derived predictors were included. Models fitted by LiDAR-derived predictors solely resulted in a mean R^2_{cv} value of 0.54. Regression coefficients for the most important LiDAR-derived predictors, according to the relative VIP, indicated a negative relation between P_{mass} and the fractional cover of trees larger than 6 m (fcover_6_60_mean) (Figs. 7, 8). Moreover, important LiDAR-derived variables indicated a negative relation of P_{mass} to the stand height (max_h_mean, perc90_h_mean, mean_h_mean) (Figs. 7, 8). Additionally, fcover_2_6_mean, related to the cover of shrubs, was the most important variable in P_{mass} models using LiDAR-derived variables solely (Fig. 8). Important hyperspectral bands were distributed across the whole spectrum with a pronounced peak around 730 nm (Fig. 4). The permutation of the calibration data according to the main forest types revealed that the success of N_{mass} and P_{mass} models was strongly dependent on two forest types being included (Fig. 9). N_{mass} models showed poor predictive performances when *P. sylvestris* stands were not included in the calibration dataset. Similarly, the absence of *P. serotina* dominated stands resulted in poor predictive performance of P_{mass} models. This observation was consistent regardless of whether hyperspectral or LiDAR data were used as predictors. Additionally, model performances were strongly influenced by the variance in canopy

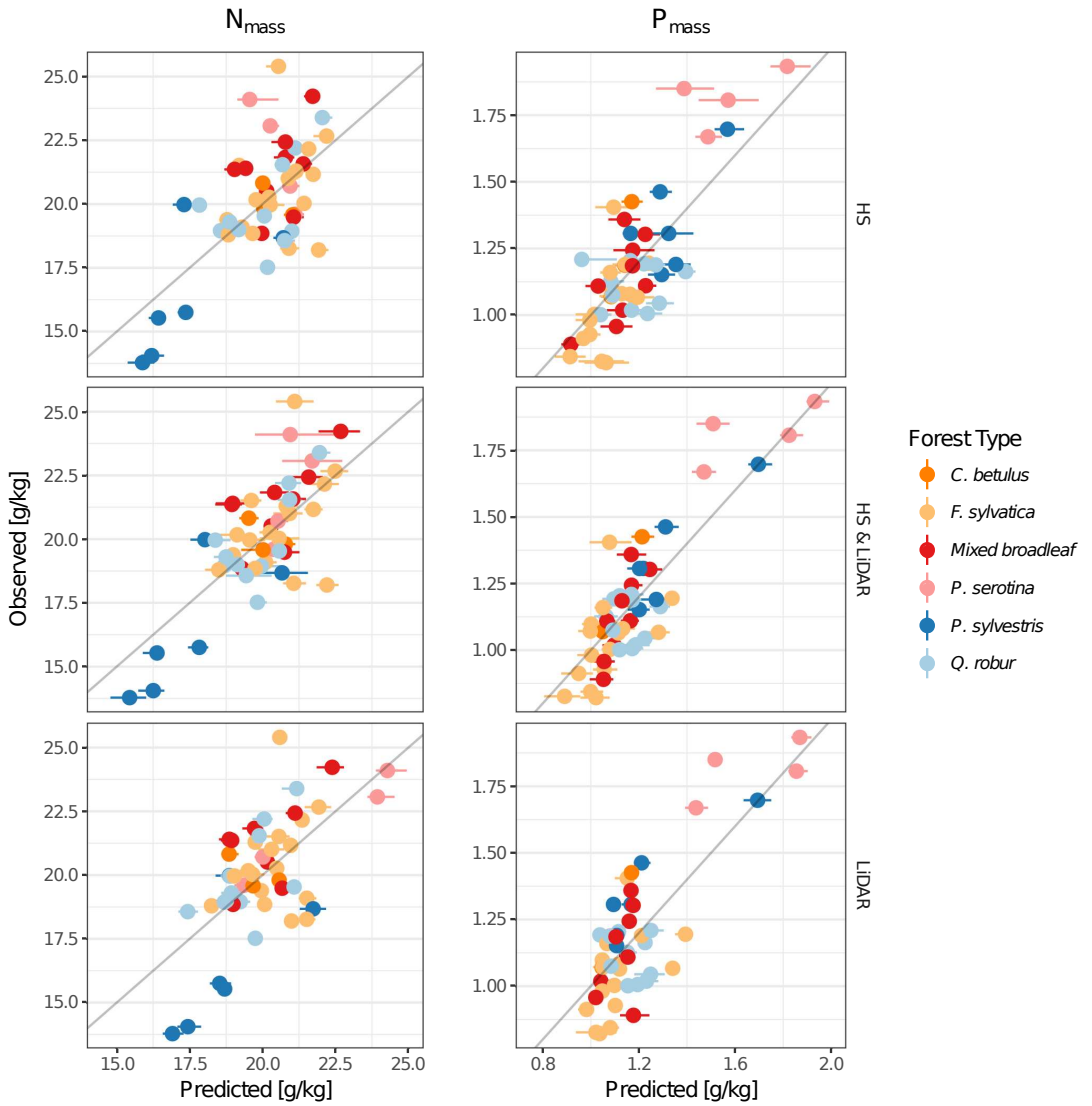

Figure 2 Mean predicted values resulting from 200 model predictions displayed against observed values for N_{mass} and P_{mass} of 50 field plots. Error bars represent lower and upper quantiles of the predictions. The figures show results from models using hyperspectral bands (HS, top), LiDAR-derived predictors (LiDAR, bottom) and a combination of both (HS & LiDAR, middle). The coloring highlights different forest types represented by dominant tree species.

height and gap fraction of field plots included in each data permutation (Fig. 10). P_{mass} models performed better with increasing variance in both structural properties. This contrasted with N_{mass} where the performance of imaging spectroscopy models decreased with increasing variation in canopy height and gap fraction. The performance of N_{mass} models was less affected by structural variation, when including LiDAR-derived variables (Fig. 10).

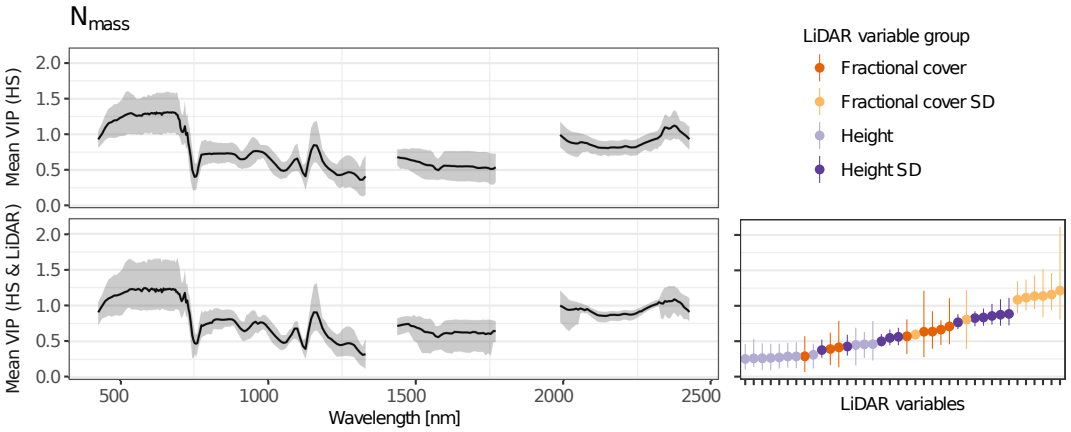

Figure 3 Mean VIP (Variable Importance in Projection) values of hyperspectral bands and LiDAR-derived variables resulting from 200 PLSR models for the prediction of N_{mass}. The top panel is showing the results from models using hyperspectral bands only, bottom panels display results from models using a combination of hyperspectral bands and LiDAR-derived predictors. Gray areas indicate the range between the 10th and the 90th percentiles. The bottom right panel is displaying mean VIP values of used LIDAR variables. For simplification LIDAR variables were grouped into four classes representing the vegetation cover (Fractional cover), the horizontal variability of vegetation cover (Fractional cover SD), LiDAR height metrics (Height), and the horizontal variability of LiDAR height metrics (Height SD).

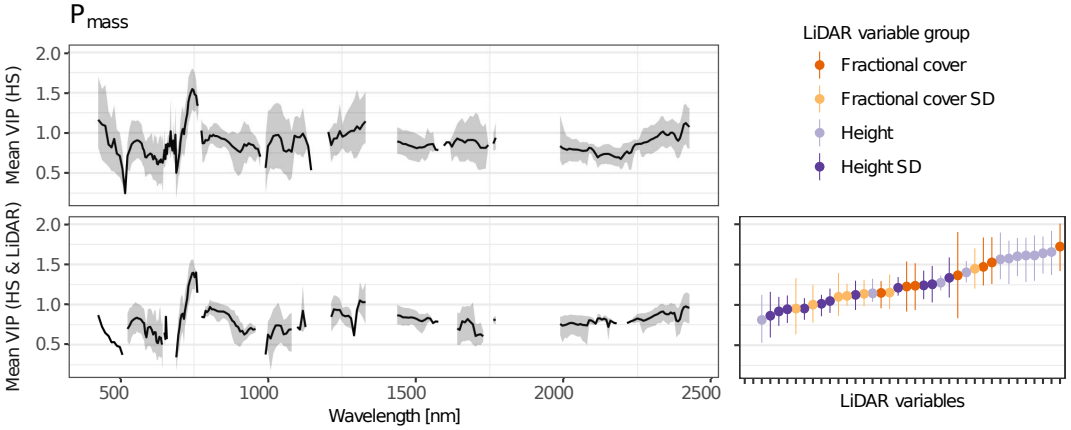

Figure 4 Mean VIP (Variable Importance in Projection) values of hyperspectral bands and LiDAR-derived variables resulting from 200 PLSR models for the prediction of P_{mass}. The top panel is showing the results from models using hyperspectral bands only, bottom panels display results from models using a combination of hyperspectral bands and LiDAR-derived predictors. Gray areas indicate the range between the 10th and the 90th percentiles. The bottom right panel is displaying mean VIP values of used LIDAR variables. For simplification LIDAR-derived variables were grouped into four classes representing the vegetation cover (Fractional cover), the horizontal variability of vegetation cover (Fractional cover SD), LiDAR height metrics (Height), and the horizontal variability of LiDAR height metrics (Height SD).

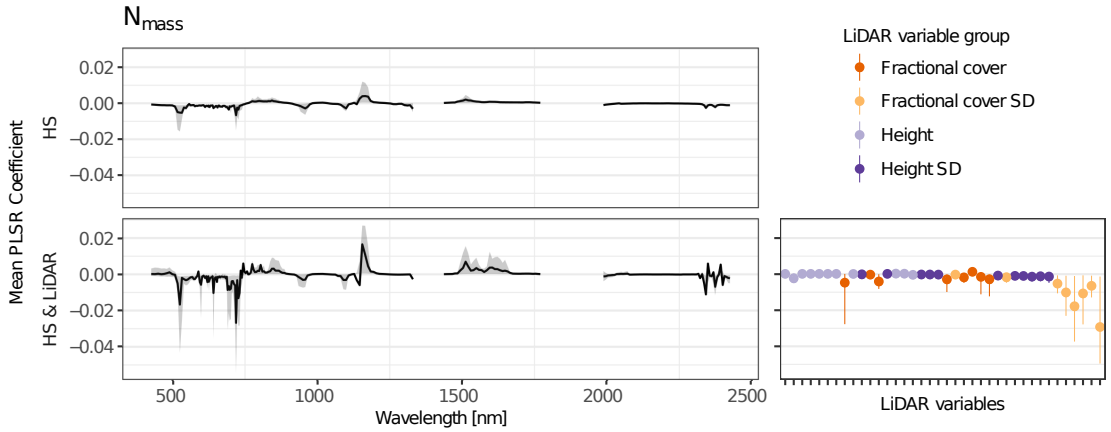

Figure 5 Mean PLSR Coefficients of hyperspectral bands and LiDAR-variables resulting from 200 model calculations for predicting N_{mass}. The top panel is showing the results from models using hyperspectral bands only, bottom panels display results from models using a combination of hyperspectral bands and LiDAR-derived variables. Gray areas indicate the range between the 10th and the 90th percentile. The bottom right panel is displaying mean PLSR coefficients of used LiDAR-derived variables. For simplification LiDAR-derived variables were grouped into four classes representing the vegetation cover (Fractional cover), the horizontal variability of vegetation cover (Fractional cover SD), LiDAR height metrics (Height), and the horizontal variability of LiDAR height metrics (Height SD). LiDAR variables are displayed in ascending order by variable importance.

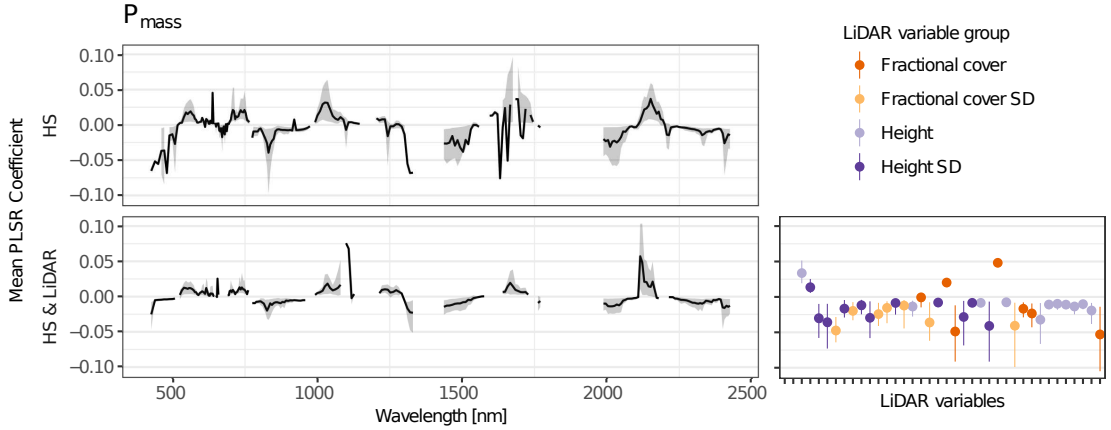

Figure 6 Mean PLSR Coefficients of hyperspectral bands and LiDAR-derived variables resulting from 200 model calculations for predicting P_{mass}. The top panel is showing the results from models using hyperspectral bands only, bottom panels display the results from models using a combination of hyperspectral bands and LiDAR-derived variables. Gray areas indicate the range between the 10 th and the 90 th percentile. The bottom right panel is displaying mean PLSR Coefficients of used LiDAR-derived variables. For simplification LiDAR-derived variables were grouped into four classes representing the vegetation cover (Fractional cover), the horizontal variability of vegetation cover (Fractional cover SD), LiDAR height metrics (Height), and the horizontal variability of LiDAR height metrics (Height SD). LiDAR variables are displayed in ascending order by variable importance.

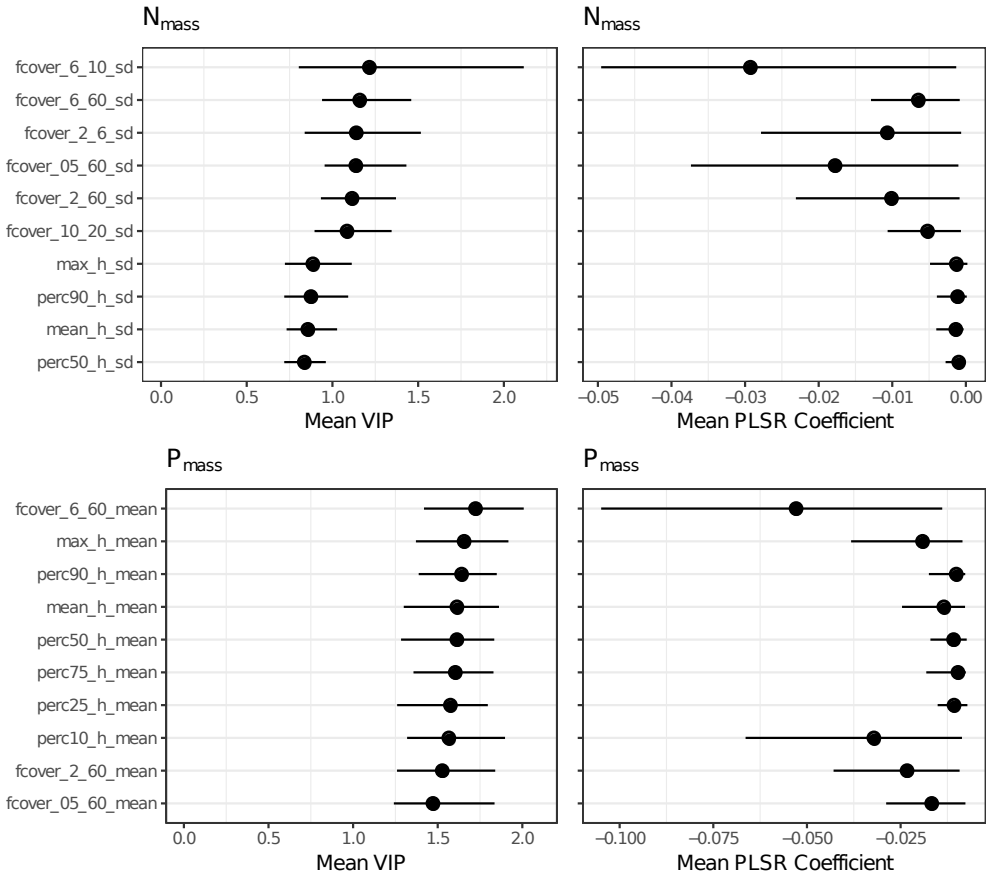

Figure 7 Mean VIP values (left) and mean PLSR coefficients (right) resulting from 200 PLSR models for the prediction of N_{mass} (top) and P_{mass} (bottom) for the ten most important LiDAR-derived variables in models using a combination of hyperspectral bands and LiDAR-derived as predictors. Error bars indicate the range between the 10th and 90th percentile.

4 Discussion

In this study we showed that LiDAR-derived information on canopy structure improved predictions of N_{mass} and P_{mass} based imaging spectroscopy instructurally heterogeneous forest stands. This finding is in accordance with previous studies using optical remote sensing data, which report a strong contribution of NIR reflectance for the prediction of N_{mass} in forest canopies (e.g. Martin et al., 2008; Ollinger et al., 2008; Wang et al., 2016)), that can be attributed to canopy structural properties (Knyazikhin et al., 2013; Ollinger, 2011). Similarly, Badgley et al. (2017) found gross primary production on a global level to be strongly related to structure-sensitive NIR reflectance. These results point at the existence of functional links between the biochemical and structural composition of forest canopies.

An ecological explanation of such linkages follows from the economic theory (Bloom et al., 1985). The economic theory states that investments in the photosynthetic ma-

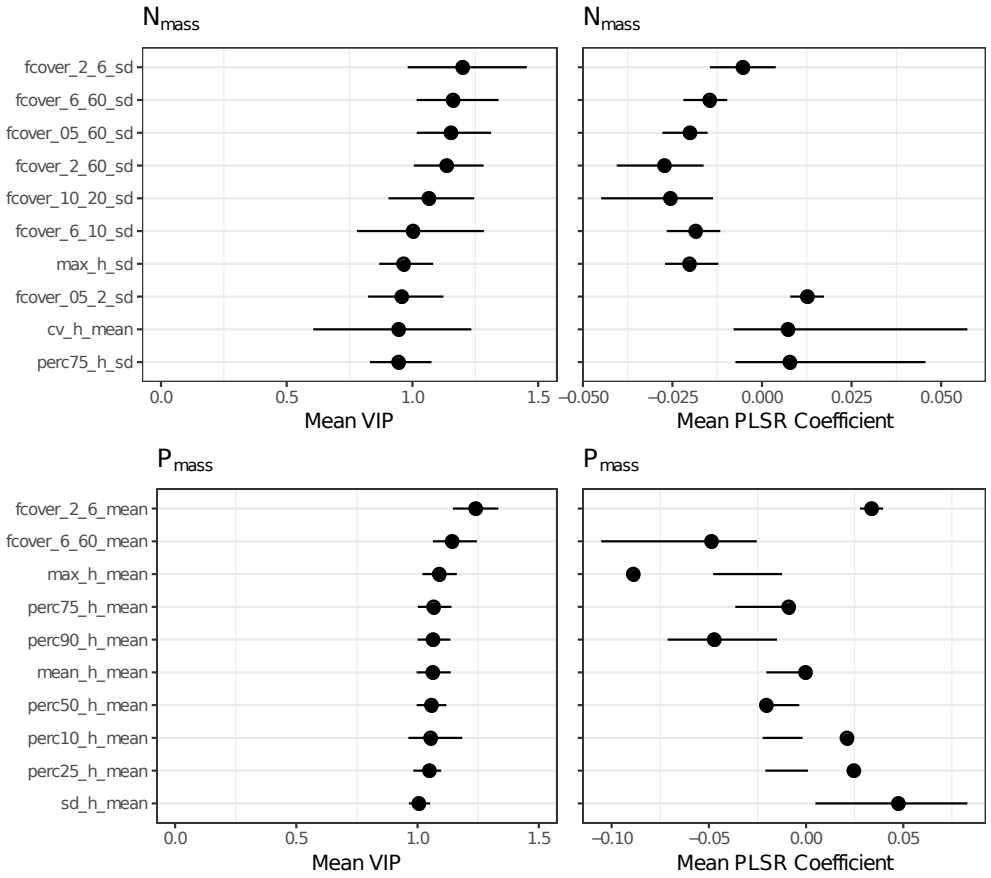

Figure 8 Mean VIP values (left) and mean PLSR coefficients (right) resulting from 200 PLSR models for the prediction of N_{mass} (top) and P_{mass} (bottom) for the ten most important LiDAR-derived variables in models using LiDAR-derived predictors only. Error bars indicate the range between the 10th and 90th percentiles.

chinery of plants will be realized only when the benefit of these investments exceeds the anticipated costs. As a result, plant traits with small cost-to-benefit relationship are favored under resource limitation, leading to a functional convergence of structural and physiological traits. At the leaf level, for example, the negative correlation between leaf mass per area and leaf nitrogen or phosphorus concentration can be attributed to functional convergence (Díaz et al., 2016; Shipley et al., 2006; Wright et al., 2004). Ecological theory suggests that, similar to the leaf level, functional convergence can also be expected at the canopy level (Field, 1991) leading to linkages between structural and biochemical canopy properties. In temperate and boreal forest ecosystems, links between structure and biochemistry are expressed at both the leaf and the canopy level. For example, broadleaved and coniferous trees show notable structural differences at the canopy level which are expressed in different crown geometry, branching architecture and leaf angle distribution (Ollinger, 2011). Both, leaf and canopy structural prop-

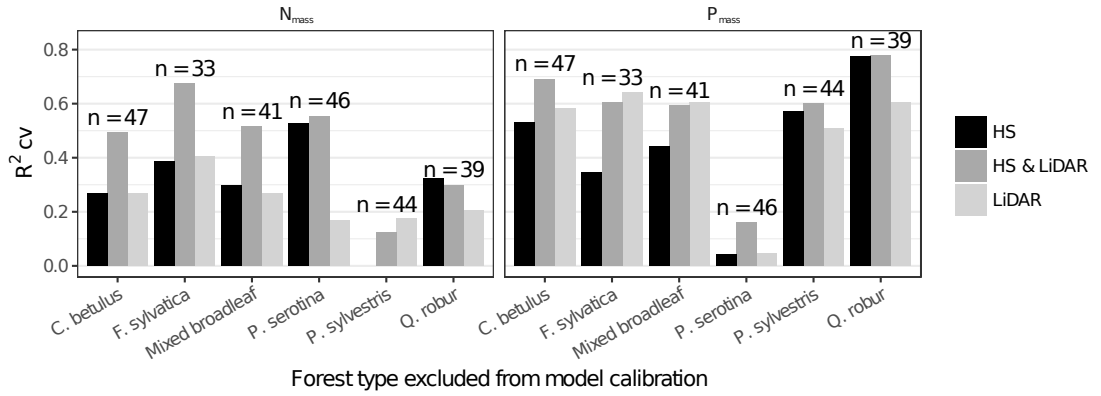

Figure 9 Predictive performances of N_{mass} and P_{mass} models using permuted calibration datasets according to occurring forest types. In each data permutation one forest type was excluded from the calibration dataset. Numbers above the bars represent the number of field plots included in each calibration dataset. HS: models using hyperspectral data; HS & LiDAR: models using a combination of hyperspectral and LiDAR data; LiDAR: models using LiDAR data only.

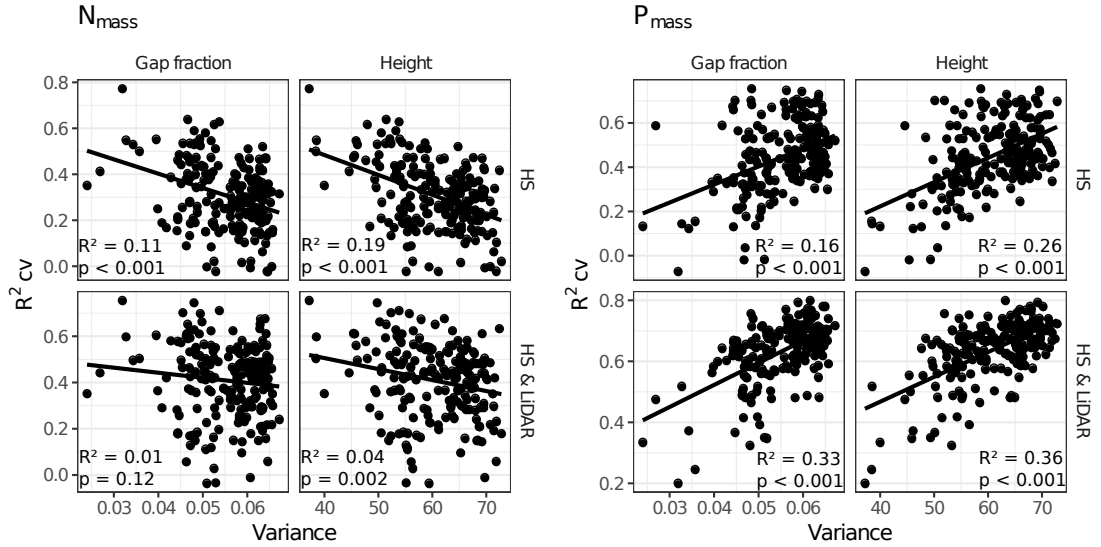

Figure 10 Predictive performances of N_{mass} and P_{mass} models depending on the variance of canopy gap fraction and canopy height included in the calibration dataset, Points represent the results from 200 model repetitions using permuted calibration data. Lines and values in each panel represent results from univariate linear regression between displayed variables. Top panels are showing the results from models using imaging spectroscopy data (HS) only, bottom panels the results from models using a combination of imaging spectroscopy and LiDAR data.

erties have shown to influence spectral reflectance in similar ways, resulting in higher reflectance of broadleaved canopies (Knyazikhin et al., 2013; Ollinger, 2011). At the same time, broadleaved trees are characterized by higher N_{mass} compared to coniferous tree species (Güsewell, 2004; Han et al., 2005; McNeil et al., 2008; Serbin et al.,

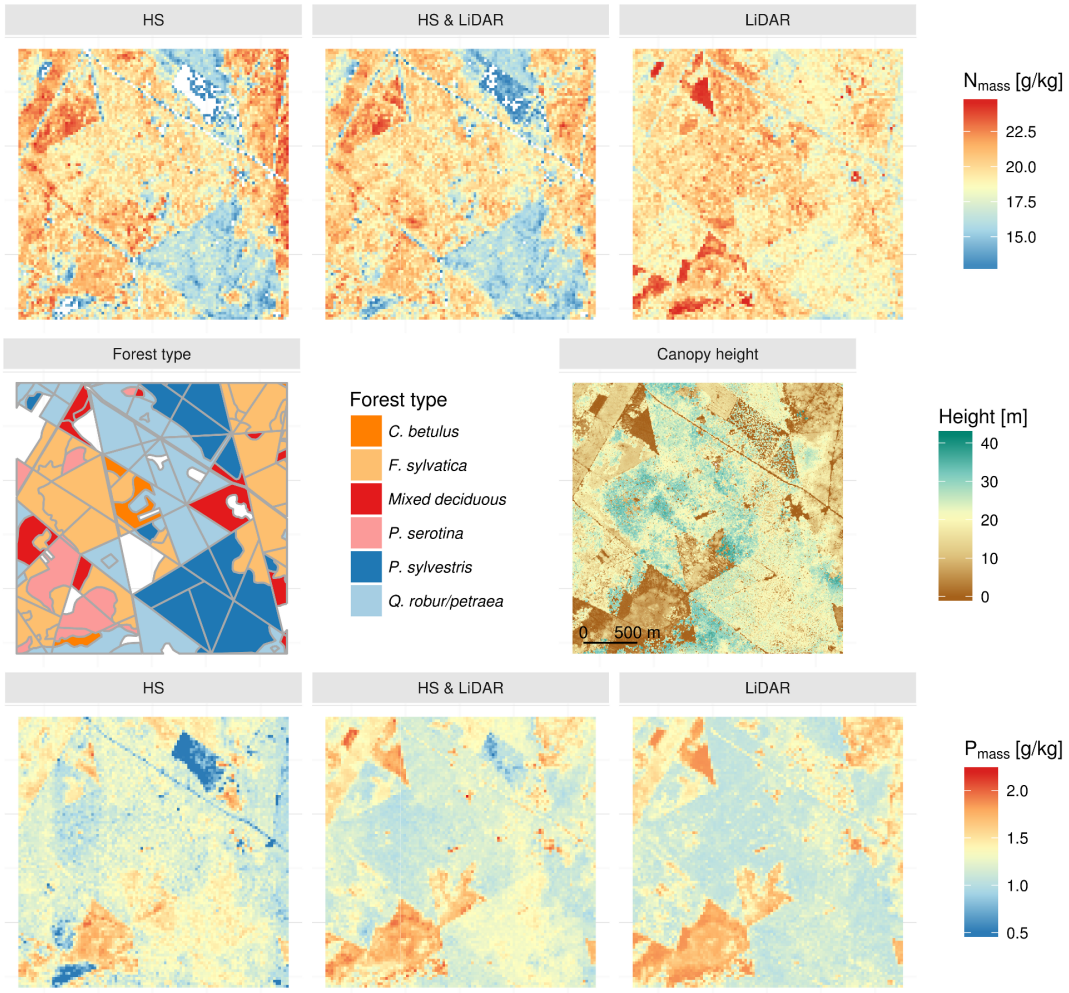

Figure 11 Map sections showing forest types represented by their dominant tree species, a canopy height model (both in the middle) and median predictions of canopy level N_{mass} (top) and P_{mass} (bottom) from models using hyperspectral bands (HS), LiDAR-derived predictors (LiDAR) or a combination of both (HS+LiDAR).

2014). Furthermore, case studies show that forest canopy N_{mass} or P_{mass} can be also related to other structural properties, such as stand density, above ground biomass or crown-closure (Craven et al., 2015; Gökkaya et al., 2015; Sardans and Peñuelas, 2015; Vilà-Cabrera et al., 2015).

In the specific context of this study, the success of N_{mass} and P_{mass} predictions was strongly dependent on the presence of two forest types that exhibited biochemical and structural differences compared to the co-occuring forest types. N_{mass} predictions depended on the presence of *P. sylvestris* stands in the calibration dataset. *Pinus sylvestris* was the only coniferous species in our study and was characterized by significantly lower N_{mass} than all other species. In contrast, P_{mass} predictions were mainly driven by *P.*

serotina, which was the species characterized by the highest P_{mass} concentrations in our study area. Structural differences between *P. serotina* and the other tree species in our study area mainly arise from its growth strategy and habitat preferences. *Prunus serotina* is an early successional tree species with significantly smaller growth heights compared to other tree species predominant in our study area. *Prunus serotina* is often a dominant species in young stands and often occurs in mature stands with sparse canopies or in canopy gaps. Our results suggest that species differences in structural and/or optical properties can serve as a surrogate to predict canopy chemistry using remote sensing, at least across small study extents, where differences in leaf nutrient concentrations can often be explained by differences between species (Craven et al., 2015; McNeil et al., 2008). For larger environmental gradients, differences between species are often superimposed by the high intra-specific variability of leaf biochemicals (Asner et al., 2012; Mellert and Göttlein, 2012; Vilà-Cabrera et al., 2015), which respond to strong variation in climate and soil properties (Sardans et al., 2015; Sun et al., 2015). The fact that our results were strongly dependent on the occurrence of two species is limiting the transferability of our findings to other study areas or broader spatial extents. However, functional differences (e.g. between broadleaved and coniferous species or between early and late successional species) that are manifested in structural and biochemical properties (Craven et al., 2015; Kusumoto et al., 2015; Sardans and Peñuelas, 2015; Vilà-Cabrera et al., 2015) suggest that canopy structure can serve as a surrogate for predicting biochemical properties also in different study contexts.

Mapping N_{mass}

Predicting forest canopy N_{mass} using imaging spectroscopy has a long history. Compared to previous studies, which often report good (e.g. Smith et al., 2003; Townsend et al., 2003; Wang et al., 2016) or even excellent (e.g. Martin et al., 2008; Singh et al., 2015) predictive performances, our models performed poorly. We attribute this mainly to the high structural diversity of the forest stands used for model calibration. This high structural diversity was, for example, expressed by strong variation of LAI values even within stands of the same forest type (i.e. ranging from 1.8 to 6.1 for *F. sylvatica* stands). Canopy structure strongly affects reflectance (Gerard and North, 1997; Rautiainen et al., 2004) and a high variability in LAI has been found to hamper predictions of leaf biochemistry at the canopy level (Asner and Martin, 2008). Furthermore, we included stands of different age classes, with canopy heights ranging between 2 and 40 meters, which also increases variation in canopy reflectance, especially in the VIS (Roberts et al., 2004). Our results suggest, that including LiDAR data can help to diminish these effects of structural heterogeneity, when mapping N_{mass} (see Fig. 10).

In part, the weak predictive performance of our N_{mass} models can be attributed to the relatively low data range of N_{mass} in our study area (cf. Asner et al., 2015; Huber et al., 2008; Martin et al., 2008; Singh et al., 2015; Smith et al., 2003; Wang et al., 2016). The range was especially low for all broadleaved species, with no significant differences between the two main species (*F. sylvatica*, *Q. robur*), which were predominant in 36 of 50 field plots (including mixed broadleaf). Furthermore, the weak model performance

can, presumably, also be attributed to the usage of mass related nitrogen measures, because spectral reflectance is more closely linked to leaf biochemistry on an area basis (Grossman et al., 1996; Roelofsen et al., 2014).

Furthermore, the performance of the N_{mass} models may also be explained by the fact that image acquisition and leaf sampling were from different years. Although previous studies suggest, that there is only low variation of N_{mass} in temperate forest species between two consecutive years and during one growing season (McKown et al., 2013; Niinemets, 2016; Reich et al., 1991; Smith et al., 2003), we cannot be 100% sure that relative differences between the species in our study area were stable between the years. Fajardo and Siefert (2016) found different patterns in N_{mass} between coniferous and broad leaf species in the course of one growing season. However, they also found that overall species rankings concerning N_{mass} were stable throughout a growing season.

The most important spectral bands selected in our N_{mass} models were situated in the visible part of the spectrum. A high contribution of the VIS region for N_{mass} prediction, using imaging spectroscopy, was also observed by Asner et al. (2015) and Singh et al. (2015). In our study the importance of bands in the VIS can be attributed to differences in reflectance between coniferous and broadleaved forest stands in this spectral region. (see supplementary material Fig. S4). These differences may arise from light absorption of chlorophyll but may also be due to other leaf pigments, like carotenoids and anthocyanins, that also have absorption characteristics in the VIS (Ollinger, 2011; Ustin et al., 2009). Moreover, structural canopy properties such as LAI or leaf angle distribution also influence reflectance in the VIS, albeit to a lower extent than leaf pigments (Jacquemoud et al., 2009). This is in accordance to previous studies that report the importance of the VIS region to discriminate between species (Fassnacht et al., 2016; Roberts et al., 2004).

VIP values indicated only a minor contribution of spectral bands located in the NIR and SWIR, which is contrary to results of previous studies using image spectroscopy (Homolová et al., 2013). According to Ollinger (2011) NIR reflectance is especially important in datasets with only little variance in the VIS reflectance. The high variance in the VIS reflectance (see supplementary material Fig. S3) observed in this study may thus be an explanation for the minor contribution of NIR and SWIR bands. Additionally, any signal in the infrared reflectance may be strongly disturbed, by the high variability of canopy gaps in the field plots used for this study (Ollinger, 2011).

For mapping N_{mass}, important LiDAR-derived variables were mainly connected to the horizontal variation of canopy cover (fcover_6_10_sd, fcover_6_60_sd, fcover_2_6_sd). These three variables represent the variation of the fractional vegetation cover between different height thresholds, in one 24 m × 24 m pixel. They can thus be interpreted as indicators for spatial heterogeneity of the canopy. The most important LiDAR-derived variable for predicting canopy level N_{mass} was the spatial variation of fractional vegetation cover between 6 and 10 m height (fcover_6_10_sd), which is related to the occurrence of shrubs or small trees in the understory. Low values either indicate little vegetation present between 6 and 10 m height, as it can be observed in mature forest stands with closed canopies, or very dense homogeneous vegetation, as it can be observed in earlier successional stages. High values indicate heterogeneous, typically old-grown forest stands with gaps that are filled by young trees. Similarly, fcover_6_60_sd is

related to the horizontal heterogeneity of the tree canopy cover, that was highest in *P. sylvestris* stands (supplementary material, Fig. S5). Moreover fcover_2_6 also was highest in *P. sylvestris* stands, indicating that LiDAR-derived variables helped to accentuate differences in N_{mass} between *P. sylvestris* and broadleaved species.

In summary, N_{mass} predictions were strongly dependent on the presence of the only coniferous tree species, *P. sylvestris*. Stands of *P. sylvestris* were characterized by lower N_{mass} and higher spatial variation of canopy cover compared to broadleaved forest stands. These structural differences could be well captured by LiDAR data (supplementary material, Fig. S5). Hence, integrating LiDAR-derived information improved models based on imaging spectroscopy data solely. The poor performance of models, using hyperspectral data solely, can be attributed to the high structural heterogeneity in the study area, in terms of LAI and stand ages. Our results suggest, that LiDAR data can help to diminish the effect of canopy heterogeneity when mapping forest N_{mass} using imaging spectroscopy.

Mapping P_{mass}

Mapping leaf phosphorus with remote sensing has received much less attention compared to N_{mass}. Earlier mapping attempts were based on hyperspectral indices (Mirik et al., 2005), radiative transfer models (Porder et al., 2005) and empirical models (Asner et al., 2015; Gökkaya et al., 2015). Gökkaya et al. (2015) achieved excellent predictive performances mapping P_{mass} in a boreal mixed forest using Hyperion imaging spectroscopy data. Asner et al. (2015) successfully mapped P_{mass} along a broad environmental gradient using airborne hyperspectral data and partial least squares regression. Contrary to N_{mass}, P_{mass} has no characteristic absorption features in the used wavelength range and thus the success of mapping P_{mass} can be rather attributed to correlations to other canopy properties. For many plant species, P_{mass} is positively correlated with N_{mass} (Elser et al., 2010; Güsewell, 2004) or leaf mass per area (Wright et al., 2004). For temperate tree species, Sardans et al. (2015) found a negative correlation between above ground biomass and leaf N:P ratio, due to higher P retention with increasing age.

Important bands for the prediction of P_{mass} were located throughout the whole range of the spectra. Asner et al. (2015) and Gökkaya et al. (2015) found similar results with important bands located in the VIS, SWIR and NIR regions. The most important selected LiDAR-derived variables were related to the cover of shrubs and the cover of trees (fcover_2_6_mean, fcover_6_60_mean). While the shrub cover was positively related to P_{mass}, tree canopy cover had an negative relationship, both indicating higher P_{mass} in very young and very open stands. We furthermore observed a negative relation between P_{mass} and LiDAR-derived variables related to vegetation height (e.g. max_h_mean, perc90_h_mean, mean_h_mean). These variables are correlated to the mean height of all LiDAR vegetation points and indicate that taller stands are related to lower P_{mass}. The observation of higher P_{mass} in younger stands reflects the observation that earlier successional stages are often characterized by higher P_{mass} (Chai et al., 2015; Eichenberg et al., 2015). Relations between important LiDAR-derived variables and P_{mass} can also be well explained by species-specific differences within the study area. *Prunus serotina*,

for which we observed highest P_{mass} values, is a characteristic species of young and early-succesional stands in the forest of Compiègne. The observed negative relation between canopy cover and P_{mass} can also be explained by species -specific differences, particularly between *P. serotina*, *P. sylvestris* and *F. sylvatica* (see supplementary material, Fig. S5). *Fagus sylvatica*, for which we observed smallest P_{mass}, is forming most dense canopies in Mid-Europe, while *P. sylvestris*, characterized by higher P_{mass} than most of the native broadleaved species, is forming very sparse canopies. *Prunus serotina* most frequently occurred in forest stands with sparse canopy cover and good light conditions (Starfinger et al., 2003).

In summary, P_{mass} predictions were driven by one tree species occurring in young or open forest stands. Existing covariation between canopy structure and P_{mass} was better captured by LiDAR data than by imaging spectroscopy. The relative importance of structural properties for mapping P_{mass} is not surprising, as phosphorus is not expected to be directly represented in the spectral signal of plant canopies.

5 Conclusion

In this study we used a combination of imaging spectroscopy and airborne LiDAR data for mapping canopy N_{mass} and P_{mass} in a forest characterized by a high structural heterogeneity. For both, N_{mass} and P_{mass}, LiDAR-derived variables improved predictions based on imaging spectroscopy solely. This highlights the importance of structural properties for remote sensing of biochemical variation in forest canopies. For N_{mass} the poor performance of hyperspectral data alone can be attributed to the high structural heterogeneity in the study area, in terms of LAI and stand ages. LiDAR data helped to capture this heterogeneity and hence improve model performances. Both, N_{mass} and P_{mass} results were strongly influenced by the presence of only two tree species featuring structural and biochemical properties different from their co-occurring tree species. This limits the transferability of identified linkages between canopy structure and biochemistry to other study settings. However, in the case of N_{mass}, the known covariation with structural properties existing at the leaf and canopy level suggests that canopy structure used as proxy, can support the mapping of N_{mass} also for different study settings. Information on canopy structure derived from airborne LiDAR can help to understand existing functional links.

Acknowledgements

This study is part of the project DIARS (Detection of invasive plant species and assessment of their impact on ecosystem properties through remote sensing) funded by the ERA-Net BiodivERsA, with the national funders: ANR (Agence Nationale de la Recherche); BelSPO (Belgian Federal Science Policy Office); and DFG (Deutsche Forschungsgemeinschaft). Michael Ewald is funded through the DFG research grant SCHM 2153/9-1. The authors would like to thank the Office National des Forêts for granting permission for leaf sampling and for providing the airborne LiDAR data. We

also wish to thank Luc Croisé, Fabien Spicher, Anthony Viaud and Jens Warrie for their help during field work. Finally, we would like to thank the anonymous reviewers for their detailed feedback, which greatly helped to improve earlier versions of the manuscript.

References

Aerts, R., Ewald, M., Nicolas, M., Piat, J., Skowronek, S., Lenoir, J., Hattab, T., Garzón-López, C.X., Feilhauer, H., Schmidtlein, S., Rocchini, D., Decocq, G., Somers, B., Van De Kerchove, R., Denef, K., Honnay, O., 2017. Invasion by the alien tree *Prunus serotina* alters ecosystem functions in a temperate deciduous forest. Frontiers in Plant Science 8, 179. doi:10.3389/fpls.2017.00179.

Ali, A.M., Darvishzadeh, R., Skidmore, A.K., van Duren, I., 2016. Effects of canopy structural variables on retrieval of leaf dry matter content and specific leaf area from remotely sensed data. IEEE Journal of Selected Topics in Applied Earth Observations and Remote Sensing 9, 898–909. doi:10.1109/JSTARS.2015.2450762.

Asner, G.P., 1998. Biophysical and biochemical sources of variability in canopy reflectance. Remote Sensing of Environment 64, 234–253. doi:10.1016/S0034-4257(98)00014-5.

Asner, G.P., Martin, R.E., 2008. Spectral and chemical analysis of tropical forests: Scaling from leaf to canopy levels. Remote Sensing of Environment 112, 3958–3970. doi:10.1016/j.rse.2008.07.003.

Asner, G.P., Martin, R.E., Anderson, C.B., Knapp, D.E., 2015. Quantifying forest canopy traits: Imaging spectroscopy versus field survey. Remote Sensing of Environment 158, 15–27. doi:10.1016/j.rse.2014.11.011.

Asner, G.P., Martin, R.E., Suhaili, A.B., 2012. Sources of canopy chemical and spectral diversity in lowland bornean forest. Ecosystems 15, 504–517. doi:10.1007/s10021-012-9526-2.

Badgley, G., Field, C.B., Berry, J.A., 2017. Canopy near-infrared reflectance and terrestrial photosynthesis. Science Advances 3, e1602244. doi:10.1126/sciadv.1602244.

Bloom, A.J., Chapin, III, F., Mooney, H.A., 1985. resource limitation in plants-an economic analogy. Annual Review of Ecology and Systematics 16, 363–392. doi:10.1146/annurev.es.16.110185.002051.

Cade, B.S., 1997. Comparison of tree basal area and canopy cover in habitat models: subalpine forest. The Journal of Wildlife Management 61, 326–335. doi:10.2307/3802588.

Chabrerie, O., Verheyen, K., Saguez, R., Decocq, G., 2008. Disentangling relationships between habitat conditions, disturbance history, plant diversity, and American black

cherry *Prunus serotina* Ehrh.) invasion in a European temperate forest. Diversity and Distributions 14, 204–212. doi:10.1111/j.1472-4642.2007.00453.x.

Chai, Y., Yue, M., Wang, M., Xu, J., Liu, X., Zhang, R., Wan, P., 2015. Plant functional traits suggest a change in novel ecological strategies for dominant species in the stages of forest succession. Oecologia 180, 771–783. doi:10.1007/s00442-015-3483-3.

Chapin, F.S., 2003. Effects of plant traits on ecosystem and regional processes: a conceptual framework for predicting the consequences of global change. Annals of Botany 91, 455–463. doi:10.1093/aob/mcg041.

Closset-Kopp, D., Saguez, R., Decocq, G., 2010. Differential growth patterns and fitness may explain contrasted performances of the invasive *Prunus serotina* in its exotic range. Biological Invasions 13, 1341–1355. doi:10.1007/s10530-010-9893-6.

Craven, D., Hall, J.S., Berlyn, G.P., Ashton, M.S., Breugel, M.v., 2015. Changing gears during succession: shifting functional strategies in young tropical secondary forests. Oecologia 179, 293–305. doi:10.1007/s00442-015-3339-x.

Curran, P.J., Kupiec, J.A., Smith, G.M., 1997. Remote sensing the biochemical composition of a slash pine canopy. IEEE Transactions on Geoscience and Remote Sensing 35, 415–420. doi:10.1109/36.563280.

Dahlin, K.M., Asner, G.P., Field, C.B., 2013. Environmental and community controls on plant canopy chemistry in a Mediterranean-type ecosystem. Proceedings of the National Academy of Sciences 110, 6895–6900. doi:10.1073/pnas.1215513110.

Di Palo, F., Fornara, D., 2015. Soil fertility and the carbon:nutrient stoichiometry of herbaceous plant species. Ecosphere 6, 1–15. doi:10.1890/ES15-00451.1.

Díaz, S., Kattge, J., Cornelissen, J.H.C., Wright, I.J., Lavorel, S., Dray, S., Reu, B., Kleyer, M., Wirth, C., Colin Prentice, I., Garnier, E., Bönisch, G., Westoby, M., Poorter, H., Reich, P.B., Moles, A.T., Dickie, J., Gillison, A.N., Zanne, A.E., Chave, J., Joseph Wright, S., Sheremet'ev, S.N., Jactel, H., Baraloto, C., Cerabolini, B., Pierce, S., Shipley, B., Kirkup, D., Casanoves, F., Joswig, J.S., Günther, A., Falczuk, V., Rüger, N., Mahecha, M.D., Gorné, L.D., 2016. The global spectrum of plant form and function. Nature 529, 167–171. doi:10.1038/nature16489.

Eichenberg, D., Trogisch, S., Huang, Y., He, J.S., Bruelheide, H., 2015. Shifts in community leaf functional traits are related to litter decomposition along a secondary forest succession series in subtropical China. Journal of Plant Ecology 8, 401–410. doi:10.1093/jpe/rtu021.

Elser, J.J., Fagan, W.F., Kerkhoff, A.J., Swenson, N.G., Enquist, B.J., 2010. Biological stoichiometry of plant production: metabolism, scaling and ecological response to global change. New Phytologist 186, 593–608. doi:10.1111/j.1469-8137.2010.03214.x.

Ewald, M., Dupke, C., Heurich, M., Müller, J., Reineking, B., 2014. LiDAR remote sensing of forest structure and GPS telemetry data provide insights on winter habitat selection of european roe deer. Forests 5, 1374–1390. doi:10.3390/f5061374.

Fajardo, A., Siefert, A., 2016. Phenological variation of leaf functional traits within species. Oecologia 180, 951–959. doi:10.1007/s00442-016-3545-1.

Fassnacht, F.E., Hartig, F., Latifi, H., Berger, C., Hernández, J., Corvalán, P., Koch, B., 2014. Importance of sample size, data type and prediction method for remote sensing-based estimations of aboveground forest biomass. Remote Sensing of Environment 154, 102–114. doi:10.1016/j.rse.2014.07.028.

Fassnacht, F.E., Latifi, H., Stereńczak, K., Modzelewska, A., Lefsky, M., Waser, L.T., Straub, C., Ghosh, A., 2016. Review of studies on tree species classification from remotely sensed data. Remote Sensing of Environment 186, 64–87. doi:10.1016/j.rse.2016.08.013.

Feilhauer, H., Asner, G.P., Martin, R.E., Schmidtlein, S., 2010. Brightness-normalized partial least squares regression for hyperspectral data. Journal of Quantitative Spectroscopy and Radiative Transfer 111, 1947–1957. doi:10.1016/j.jqsrt.2010.03.007.

Garnier, E., Lavorel, S., Ansquer, P., Castro, H., Cruz, P., Dolezal, J., Eriksson, O., Fortunel, C., Freitas, H., Golodets, C., Grigulis, K., Jouany, C., Kazakou, E., Kigel, J., Kleyer, M., Lehsten, V., Lepš, J., Meier, T., Pakeman, R., Papadimitriou, M., Papanastasis, V.P., Quested, H., Quétier, F., Robson, M., Roumet, C., Rusch, G., Skarpe, C., Sternberg, M., Theau, J.P., Thébault, A., Vile, D., Zarovali, M.P., 2007. Assessing the effects of land-use change on plant traits, communities and ecosystem functioning in grasslands: a standardized methodology and lessons from an application to 11 European sites. Annals of Botany 99, 967–985. doi:10.1093/aob/mcl215.

Gerard, F.F., North, P.R.J., 1997. Analyzing the effect of structural variability and canopy gaps on forest BRDF using a geometric-optical model. Remote Sensing of Environment 62, 46–62. doi:10.1016/S0034-4257(97)00070-9.

Gill, S.J., Biging, G.S., Murphy, E.C., 2000. Modeling conifer tree crown radius and estimating canopy cover. Forest Ecology and Management 126, 405–416. doi:10.1016/S0378-1127(99)00113-9.

Grassi, G., Vicinelli, E., Ponti, F., Cantoni, L., Magnani, F., 2005. Seasonal and inter-annual variability of photosynthetic capacity in relation to leaf nitrogen in a deciduous forest plantation in northern Italy. Tree Physiology 25, 349–360.

Grossman, Y.L., Ustin, S.L., Jacquemoud, S., Sanderson, E.W., Schmuck, G., Verdebout, J., 1996. Critique of stepwise multiple linear regression for the extraction of leaf biochemistry information from leaf reflectance data. Remote Sensing of Environment 56, 182–193. doi:10.1016/0034-4257(95)00235-9.

Gökkaya, K., Thomas, V., Noland, T.L., McCaughey, H., Morrison, I., Treitz, P., 2015. Prediction of macronutrients at the canopy level using spaceborne imaging spectroscopy and LiDAR data in a mixedwood boreal forest. Remote Sensing 7, 9045–9069. doi:10.3390/rs70709045.

Güsewell, S., 2004. N : P ratios in terrestrial plants: variation and functional significance. New Phytologist 164, 243–266. doi:10.1111/j.1469-8137.2004.01192.x.

Han, W., Fang, J., Guo, D., Zhang, Y., 2005. Leaf nitrogen and phosphorus stoichiometry across 753 terrestrial plant species in China. New Phytologist 168, 377–385. doi:10.1111/j.1469-8137.2005.01530.x.

Homolová, L., Malenovský, Z., Clevers, J.G.P.W., García-Santos, G., Schaepman, M.E., 2013. Review of optical-based remote sensing for plant trait mapping. Ecological Complexity 15, 1–16. doi:10.1016/j.ecocom.2013.06.003.

Huber, S., Kneubühler, M., Psomas, A., Itten, K., Zimmermann, N.E., 2008. Estimating foliar biochemistry from hyperspectral data in mixed forest canopy. Forest Ecology and Management 256, 491–501. doi:10.1016/j.foreco.2008.05.011.

Jacquemoud, S., Verhoef, W., Baret, F., Bacour, C., Zarco-Tejada, P.J., Asner, G.P., François, C., Ustin, S.L., 2009. PROSPECT+SAIL models: A review of use for vegetation characterization. Remote Sensing of Environment 113, S56–S66. doi:10.1016/j.rse.2008.01.026.

Jonard, M., Fürst, A., Verstraeten, A., Thimonier, A., Timmermann, V., Potočić, N., Waldner, P., Benham, S., Hansen, K., Merilä, P., Ponette, Q., de la Cruz, A.C., Roskams, P., Nicolas, M., Croisé, L., Ingerslev, M., Matteucci, G., Decinti, B., Bascietto, M., Rautio, P., 2015. Tree mineral nutrition is deteriorating in Europe. Global Change Biology 21, 418–430. doi:10.1111/gcb.12657.

Kimberley, A., Alan Blackburn, G., Duncan Whyatt, J., Smart, S.M., 2014. Traits of plant communities in fragmented forests: the relative influence of habitat spatial configuration and local abiotic conditions. Journal of Ecology 102, 632–640. doi:10.1111/1365-2745.12222.

Knyazikhin, Y., Schull, M.A., Stenberg, P., Mõttus, M., Rautiainen, M., Yang, Y., Marshak, A., Carmona, P.L., Kaufmann, R.K., Lewis, P., Disney, M.I., Vanderbilt, V., Davis, A.B., Baret, F., Jacquemoud, S., Lyapustin, A., Myneni, R.B., 2013. Hyperspectral remote sensing of foliar nitrogen content. Proceedings of the National Academy of Sciences 110, E185–E192. doi:10.1073/pnas.1210196109.

Kokaly, R.F., Asner, G.P., Ollinger, S.V., Martin, M.E., Wessman, C.A., 2009. Characterizing canopy biochemistry from imaging spectroscopy and its application to ecosystem studies. Remote Sensing of Environment 113, 78–91. doi:10.1016/j.rse.2008.10.018.

Korhonen, L., Korpela, I., Heiskanen, J., Maltamo, M., 2011. Airborne discrete-return LIDAR data in the estimation of vertical canopy cover, angular canopy closure and leaf area index. Remote Sensing of Environment 115, 1065–1080. doi:10.1016/j.rse.2010.12.011.

Kusumoto, B., Shiono, T., Miyoshi, M., Maeshiro, R., Fujii, S.j., Kuuluvainen, T., Kubota, Y., 2015. Functional response of plant communities to clearcutting: management impacts differ between forest vegetation zones. Journal of Applied Ecology 52, 171–180. doi:10.1111/1365-2664.12367.

Lamarque, P., Lavorel, S., Mouchet, M., Quétier, F., 2014. Plant trait-based models identify direct and indirect effects of climate change on bundles of grassland ecosystem services. Proceedings of the National Academy of Sciences 111, 13751–13756. doi:10.1073/pnas.1216051111.

Lavorel, S., Grigulis, K., Lamarque, P., Colace, M.P., Garden, D., Girel, J., Pellet, G., Douzet, R., 2011. Using plant functional traits to understand the landscape distribution of multiple ecosystem services. Journal of Ecology 99, 135–147. doi:10.1111/j.1365-2745.2010.01753.x.

Martin, M.E., Aber, J.D., 1997. High spectral resolution remote sensing of forest canopy lignin, nitrogen, and ecosystem processes. Ecological Applications 7, 431–443. doi:10.2307/2269510.

Martin, M.E., Plourde, L.C., Ollinger, S.V., Smith, M.L., McNeil, B.E., 2008. A generalizable method for remote sensing of canopy nitrogen across a wide range of forest ecosystems. Remote Sensing of Environment 112, 3511–3519. doi:10.1016/j.rse.2008.04.008.

Masek, J.G., Hayes, D.J., Joseph Hughes, M., Healey, S.P., Turner, D.P., 2015. The role of remote sensing in process-scaling studies of managed forest ecosystems. Forest Ecology and Management 355, 109–123. doi:10.1016/j.foreco.2015.05.032.

McKown, A.D., Guy, R.D., Azam, M.S., Drewes, E.C., Quamme, L.K., 2013. Seasonality and phenology alter functional leaf traits. Oecologia 172, 653–665. doi:10.1007/s00442-012-2531-5.

McNeil, B.E., Read, J.M., Sullivan, T.J., McDonnell, T.C., Fernandez, I.J., Driscoll, C.T., 2008. The spatial pattern of nitrogen cycling in the adirondack park, New York. Ecological Applications 18, 438–452. doi:10.1890/07-0276.1.

Melillo, J.M., Aber, J.D., Muratore, J.F., 1982. Nitrogen and lignin control of hardwood leaf litter decomposition dynamics. Ecology 63, 621–626. doi:10.2307/1936780.

Mellert, K.H., Göttlein, A., 2012. Comparison of new foliar nutrient thresholds derived from van den Burg's literature compilation with established central European references. European Journal of Forest Research 131, 1461–1472. doi:10.1007/s10342-012-0615-8.

Mirik, M., Norland, J.E., Crabtree, R.L., Biondini, M.E., 2005. Hyperspectral one-meter-resolution remote sensing in Yellowstone National Park, Wyoming: I. forage nutritional values. Rangeland Ecology & Management 58, 452–458. doi:10.2111/04-17.1.

Niinemets, U., 2016. Leaf age dependent changes in within-canopy variation in leaf functional traits: a meta-analysis. Journal of Plant Research 129, 313–338. doi:10.1007/s10265-016-0815-2.

Ollinger, S.V., 2011. Sources of variability in canopy reflectance and the convergent properties of plants. New Phytologist 189, 375–394. doi:10.1111/j.1469-8137.2010.03536.x.

Ollinger, S.V., Richardson, A.D., Martin, M.E., Hollinger, D.Y., Frolking, S.E., Reich, P.B., Plourde, L.C., Katul, G.G., Munger, J.W., Oren, R., Smith, M.L., U, K.T.P., Bolstad, P.V., Cook, B.D., Day, M.C., Martin, T.A., Monson, R.K., Schmid, H.P., 2008. Canopy nitrogen, carbon assimilation, and albedo in temperate and boreal forests: Functional relations and potential climate feedbacks. Proceedings of the National Academy of Sciences 105, 19336–19341. doi:10.1073/pnas.0810021105.

Ollinger, S.V., Smith, M.L., Martin, M.E., Hallett, R.A., Goodale, C.L., Aber, J.D., 2002. Regional variation in foliar chemistry and N cycling among forests of diverse history and composition. Ecology 83, 339–355. doi:10.1890/0012-9658(2002)083[0339:RVIFCA]2.0.CO;2.

Porder, S., Asner, G.P., Vitousek, P.M., 2005. Ground-based and remotely sensed nutrient availability across a tropical landscape. Proceedings of the National Academy of Sciences of the United States of America 102, 10909–10912. doi:10.1073/pnas.0504929102.

Pullanagari, R.R., Kereszturi, G., Yule, I.J., 2016. Mapping of macro and micro nutrients of mixed pastures using airborne AisaFENIX hyperspectral imagery. ISPRS Journal of Photogrammetry and Remote Sensing 117, 1–10. doi:10.1016/j.isprsjprs.2016.03.010.

R Core Team, 2016. R: A Language and Environment for Statistical Computing. R Foundation for Statistical Computing, Vienna, Austria. URL: https://www.R-project.org/.

Rautiainen, M., Stenberg, P., Nilson, T., Kuusk, A., 2004. The effect of crown shape on the reflectance of coniferous stands. Remote Sensing of Environment 89, 41–52. doi:10.1016/j.rse.2003.10.001.

Reich, P.B., 2012. Key canopy traits drive forest productivity. Proceedings of the Royal Society of London B: Biological Sciences 279, 2128–2134. doi:10.1098/rspb.2011.2270.

Reich, P.B., Walters, M.B., Ellsworth, D.S., 1991. Leaf age and season influence the relationships between leaf nitrogen, leaf mass per area and photosynthesis in maple and oak trees. Plant, Cell & Environment 14, 251–259. doi:10.1111/j.1365-3040.1991.tb01499.x.

Roberts, D.A., Ustin, S.L., Ogunjemiyo, S., Greenberg, J., Dobrowski, S.Z., Chen, J., Hinckley, T.M., 2004. Spectral and structural measures of northwest forest vegetation at leaf to landscape scales. Ecosystems 7, 545–562. doi:10.1007/s10021-004-0144-5.

Roelofsen, H.D., van Bodegom, P.M., Kooistra, L., Witte, J.P.M., 2014. Predicting leaf traits of herbaceous species from their spectral characteristics. Ecology and Evolution 4, 706–719. doi:10.1002/ece3.932.

Sardans, J., Janssens, I.A., Alonso, R., Veresoglou, S.D., Rillig, M.C., Sanders, T.G., Carnicer, J., Filella, I., Farré-Armengol, G., Peñuelas, J., 2015. Foliar elemental composition of European forest tree species associated with evolutionary traits and present environmental and competitive conditions. Global Ecology and Biogeography 24, 240–255. doi:10.1111/geb.12253.

Sardans, J., Peñuelas, J., 2015. Trees increase their P:N ratio with size. Global Ecology and Biogeography 24, 147–156. doi:10.1111/geb.12231.

Schlerf, M., Atzberger, C., Hill, J., Buddenbaum, H., Werner, W., Schüler, G., 2010. Retrieval of chlorophyll and nitrogen in Norway spruce (*Picea abies* L. Karst.) using imaging spectroscopy. International Journal of Applied Earth Observation and Geoinformation 12, 17–26. doi:10.1016/j.jag.2009.08.006.

Schmidtlein, S., Feilhauer, H., Bruelheide, H., 2012. Mapping plant strategy types using remote sensing. Journal of Vegetation Science 23, 395–405. doi:10.1111/j.1654-1103.2011.01370.x.

Serbin, S.P., Singh, A., McNeil, B.E., Kingdon, C.C., Townsend, P.A., 2014. Spectroscopic determination of leaf morphological and biochemical traits for northern temperate and boreal tree species. Ecological Applications 24, 1651–1669. doi:10.1890/13-2110.1.

Serrano, L., Peñuelas, J., Ustin, S.L., 2002. Remote sensing of nitrogen and lignin in Mediterranean vegetation from AVIRIS data: Decomposing biochemical from structural signals. Remote Sensing of Environment 81, 355–364. doi:10.1016/S0034-4257(02)00011-1.

Shipley, B., Lechowicz, M.J., Wright, I., Reich, P.B., 2006. Fundamental trade-offs generating the worldwide leaf economics spectrum. Ecology 87, 535–541. doi:10.1890/05-1051.

Simic, A., Chen, J.M., Noland, T.L., 2011. Retrieval of forest chlorophyll content using canopy structure parameters derived from multi-angle data: the measurement con-

cept of combining nadir hyperspectral and off-nadir multispectral data. International Journal of Remote Sensing 32, 5621–5644. doi:10.1080/01431161.2010.507257.

Singh, A., Serbin, S.P., McNeil, B.E., Kingdon, C.C., Townsend, P.A., 2015. Imaging spectroscopy algorithms for mapping canopy foliar chemical and morphological traits and their uncertainties. Ecological Applications 25, 2180–2197. doi:10.1890/14-2098.1.

Smith, M.L., Martin, M.E., Plourde, L., Ollinger, S.V., 2003. Analysis of hyperspectral data for estimation of temperate forest canopy nitrogen concentration: comparison between an airborne (AVIRIS) and a spaceborne (Hyperion) sensor. IEEE Transactions of Geoscience and Remote Sensing 41, 1332–1337.

Starfinger, U., Kowarik, I., Rode, M., Schepker, H., 2003. From desirable ornamental plant to pest to accepted addition to the flora? – the perception of an alien tree species through the centuries. Biological Invasions 5, 323–335. doi:10.1023/B:BINV.0000005573.14800.07.

Sterckx, S., Vreys, K., Biesemans, J., Iordache, M.D., Bertels, L., Meuleman, K., 2016. Atmospheric correction of APEX hyperspectral data. Miscellanea Geographica 20, 16–20. doi:10.1515/mgrsd-2015-0022.

Suding, K.N., Lavorel, S., Chapin, F.S., Cornelissen, J.H.C., Díaz, S., Garnier, E., Goldberg, D., Hooper, D.U., Jackson, S.T., Navas, M.L., 2008. Scaling environmental change through the community-level: a trait-based response-and-effect framework for plants. Global Change Biology 14, 1125–1140. doi:10.1111/j.1365-2486.2008.01557.x.

Sun, X., Kang, H., Kattge, J., Gao, Y., Liu, C., 2015. Biogeographic patterns of multi-element stoichiometry of *Quercus variabilis* leaves across China. Canadian Journal of Forest Research 45, 1827–1834. doi:10.1139/cjfr-2015-0110.

Talkner, U., Meiwes, K.J., Potočić, N., Seletković, I., Cools, N., Vos, B.D., Rautio, P., 2015. Phosphorus nutrition of beech (*Fagus sylvatica* L.) is decreasing in Europe. Annals of Forest Science 72, 919–928. doi:10.1007/s13595-015-0459-8.

Townsend, P.A., Foster, J.R., Chastain, R.A., Currie, W.S., 2003. Application of imaging spectroscopy to mapping canopy nitrogen in the forests of the central Appalachian Mountains using Hyperion and AVIRIS. IEEE Transactions on Geoscience and Remote Sensing 41, 1347–1354. doi:10.1109/TGRS.2003.813205.

Ustin, S.L., Gitelson, A.A., Jacquemoud, S., Schaepman, M., Asner, G.P., Gamon, J.A., Zarco-Tejada, P., 2009. Retrieval of foliar information about plant pigment systems from high resolution spectroscopy. Remote Sensing of Environment 113, S67–S77. doi:10.1016/j.rse.2008.10.019.

Vilà-Cabrera, A., Martínez-Vilalta, J., Retana, J., 2015. Functional trait variation along environmental gradients in temperate and Mediterranean trees. Global Ecology and Biogeography 24, 1377–1389. doi:10.1111/geb.12379.

Vreys, K., Iordache, M.D., Biesemans, J., Meuleman, K., 2016. Geometric correction of APEX hyperspectral data. Miscellanea Geographica 20, 11–15. doi:10.1515/mgrsd-2016-0006.

Wang, Z., Wang, T., Darvishzadeh, R., Skidmore, A.K., Jones, S., Suarez, L., Woodgate, W., Heiden, U., Heurich, M., Hearne, J., 2016. Vegetation indices for mapping canopy foliar nitrogen in a mixed temperate forest. Remote Sensing 8, 491. doi:10.3390/rs8060491.

Wilson, K.B., Baldocchi, D.D., Hanson, P.J., 2000. Spatial and seasonal variability of photosynthetic parameters and their relationship to leaf nitrogen in a deciduous forest. Tree Physiology 20, 565–578. doi:10.1093/treephys/20.9.565.

Wright, I.J., Reich, P.B., Westoby, M., Ackerly, D.D., Baruch, Z., Bongers, F., Cavender-Bares, J., Chapin, T., Cornelissen, J.H.C., Diemer, M., Flexas, J., Garnier, E., Groom, P.K., Gulias, J., Hikosaka, K., Lamont, B.B., Lee, T., Lee, W., Lusk, C., Midgley, J.J., Navas, M.L., Niinemets, U., Oleksyn, J., Osada, N., Poorter, H., Poot, P., Prior, L., Pyankov, V.I., Roumet, C., Thomas, S.C., Tjoelker, M.G., Veneklaas, E.J., Villar, R., 2004. The worldwide leaf economics spectrum. Nature 428, 821–827. doi:10.1038/nature02403.

Xiao, Y., Zhao, W., Zhou, D., Gong, H., 2014. Sensitivity analysis of vegetation reflectance to biochemical and biophysical variables at leaf, canopy, and regional scales. IEEE Transactions on Geoscience and Remote Sensing 52, 4014–4024. doi:10.1109/TGRS.2013.2278838.

Zolkos, S.G., Goetz, S.J., Dubayah, R., 2013. A meta-analysis of terrestrial aboveground biomass estimation using lidar remote sensing. Remote Sensing of Environment 128, 289–298. doi:10.1016/j.rse.2012.10.017.